IOP Publishing Measurement Science and Technology
Meas. Sci. Technol. 31 (2020) 045018 (9pp) https://doi.org/10.1088/1361-6501/ab575c

Design considerations for rotation scanning projection moiré topography

Ying Tang[1,2] **and Jubing Chen**[1,3]

[1] Department of Engineering Mechanics, Shanghai Jiao Tong University, Shanghai, People's Republic of China
[2] Shanghai-Fanuc Robotics Co., Ltd., Shanghai, People's Republic of China
[3] MOE Key Laboratory of Hydrodynamics, Shanghai Jiao Tong University, Shanghai, People's Republic of China

E-mail: jbchen@sjtu.edu.cn

Received 27 July 2019, revised 28 September 2019
Accepted for publication 13 November 2019
Published 29 January 2020

Abstract

Projection moiré topography is an optical technique for 3D surface reconstruction based on the geometric interference between two optical grids. To expand the measurement area and to maintain a high measurement resolution, a rotation scanning projection moiré profilometry technique is developed here. We present the mathematical description of an arbitrarily arranged projection moiré model, and derive the expression for phase and coordinates. On this basis, we establish a relation between the system parameters and rotation parameters, making it possible to calculate the system parameters and perform surface reconstruction for any rotation angle, using the same projection moiré model.

Keywords: moiré method, topography, rotation scanning projection moiré

(Some figures may appear in colour only in the online journal)

1. Introduction

The moiré method was first introduced ~50 years ago [1, 2]. Moiré patterns are low-frequency fringe patterns generated by the geometric interference between two grids with similar frequencies. The geometric interference, which amplifies displacement without distortion, makes the moiré method more sensitive compared with other structured light methods. Using the phase-shifting method [3–5], we can easily calculate full-field phase maps and then unwrap the phase [6–8] to calculate displacement.

In the projection moiré approach, a specimen grating is projected onto an object's surface. The measurement area can be adjusted by increasing or reducing the projection area. The projection moiré method [9, 10] is used to measure out-of-plane displacement. With a reference plane, the out-of-plane displacement can be considered as height. Owing to its advantages of being a non-contacting, high-speed, full-field-measuring, and high-resolution method, the projection moiré method is widely applied in many fields [11–16], such as detection of structural scoliosis [13] and measurement of elastic-plastic stress/strain [14, 15]. Obviously, the moiré method's resolution positively correlates with the grid frequency. Higher frequency implies smaller grating pitch, yielding larger phase changes for the same height. When measuring a large object in high resolution (for example, monitoring a satellite's antenna deformation) and prescribing adjustment for segmented components, if the measurement area is simply expanded by adjusting the zoom lens in the projection system, the system's accuracy and resolution will decrease; a way to overcome this drawback is to develop a rotation scanning measurement system.

Much research has been done on applications of structured light scanning to problems, such as three-dimensional (3D) object modeling [17], robot vision [18], and documentation of archaeological finds [19]. These scanning techniques were developed based on different structured light methods, including line-structured light and surface-structured light, and the measurement accuracy and resolution are expected to decrease in most circumstances. Taking a facial scanning system, for example, the error for the same observer is under 1 mm, while the inter-observer error is ~1.5 mm [20]. Given that surface-structured light has higher measurement efficiency, and the projection moiré method has the highest

resolution among surface structured light methods, we believe it is necessary and meaningful to develop a scanning projection moiré technique.

In our previous work, we have already built a model for an arbitrarily arranged projection moiré system, derived expressions for linking phase variation and height, presented an iterative method to calculate the height from the phase, and proposed a calibration method to calibrate the system parameters [21]. These findings are also applicable to the rotation scanning projection moiré system. Considering the structural characteristics of measurement systems, scanning projection moiré systems can be classified into two types: (i) a single-axis mode with a projection system and a receiving system placed on the same turntable, and (ii) a dual-axis mode with a projection system and a receiving system placed on two turntables. Nevertheless, the single-axis mode can be seen as a special case of the dual-axis mode, and the theory for the dual-axis mode can also be applied to the single-axis mode. The main problem that needs to be solved is how the system parameters would transform after rotation. For the sake of simplicity of the rotation scanning system, the two main parts of the rotation scanning projection moiré system (the projecting system and the receiving system) could be seen as one block, the components and configurations of which would not change in both systems. This paper first introduces the basic principle of the projection moiré topography. Next, we provide a detailed derivation of parameter transformations for the rotation scanning projection moiré technique. Finally, we describe a system-validation experiment.

2. Theory

2.1. Projection moiré topography

Figure 1 illustrates a generalized arbitrarily arranged projection moiré system. The projection system on the left bottom projects fringe pictures, and the receiving system captures pictures. The projection system can be divided into two parts: a wide-angle lens, L_1, and a 'luminous' grating, G_1. Usually G_1 is a light-emitting element in a projector, which is a digital micromirror device (DMD) showing fringe pictures. L_1 amplifies parallel fringes onto the object's surface. The fringe projection is modulated by the object's surface. The receiving system is composed of a wide-angle lens, L_2, a standard grating, G_2, and a charge-coupled device (CCD) camera linked to a computer to capture digital images behind them. L_2 images modulated fringes onto G_2, where the moiré pattern is generated. The CCD camera transforms the optical information into digital information, and all the moiré patterns on G_2 are recorded as digital images. The world coordinate system ($OXYZ$) is fixed in the reference plane, and two other coordinate systems, $O_1X_1Y_1Z_1$, and $O_2X_2Y_2Z_2$, are fixed at the lenses, with the centres of lenses O_1 and O_2 being the origin, while the lenses' axis stand for the Z_1 and Z_2 axes.

Considering an arbitrary point $A\,(x, y, z)$ in the reference plane, its coordinates in the other two coordinate systems, $O_1X_1Y_1Z_1$, and $O_2X_2Y_2Z_2$, are (x_1, y_1, z_1) and (x_2, y_2, z_2), respectively:

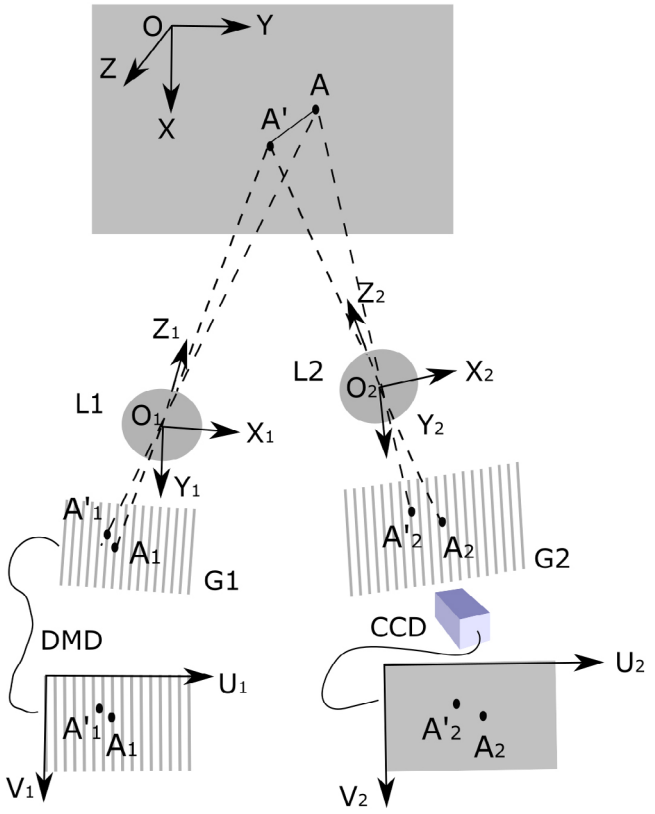

Figure 1. Schematic of the projection moiré system.

$$(x_1, y_1, z_1)^T = R_1(x, y, z)^T + T_1 \tag{1}$$

$$(x_2, y_2, z_2)^T = R_2(x, y, z)^T + T_2. \tag{2}$$

R_1, R_2 are unit orthogonal rotation matrices. T_1, T_2 are translation vectors.

A_1 and A_2 are the corresponding points of A on the two gratings. Regarding the projection system as an inverse camera, and considering the receiving system as a whole, the pixel coordinate (u_1, v_1) of A_1 in the fringe picture, and the pixel coordinate (u_2, v_2) of A_2 in the picture captured by the CCD are

$$(u_1, v_1, 1)^T = K_1\left(\frac{x_1}{z_1}, \frac{y_1}{z_1}, 1\right)^T \tag{3}$$

$$(u_2, v_2, 1)^T = K_2\left(\frac{x_2}{z_2}, \frac{y_2}{z_2}, 1\right)^T. \tag{4}$$

K_1 and K_2 are intrinsic parameters of the projection and the receiving systems.

The phase of the moiré pattern is the difference between the two gratings:

$$\varphi_{1(x,y,z)} = \left(\frac{2\pi u_1}{p_1} + \varphi_{10}\right) - \left(\frac{2\pi u_2}{p_2} + \varphi_{20}\right). \tag{5}$$

p_1 and p_2 are the equivalent pitches of gratings G_1 and G_2 in the pixel. p_1 is the period of the fringe pattern we project onto the reference plane. $p_2 = p \times c$, where p is the pitch of the standard grating G_2, and c is the scale factor of the CCD

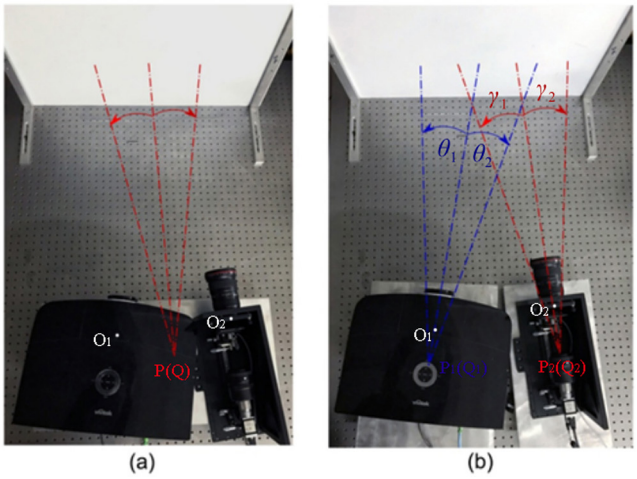

Figure 2. Two types of rotation scanning projection moiré system: (a) single-axis mode, (b) dual-axis mode.

camera. φ_{10} and φ_{20} are the initial phases of gratings G_1 and G_2.

Removing the reference plane and putting an object in the measurement area, point $A\,(x, y, z)$ becomes $A'\,(x, y, z+h\,(x, y))$. Its phase is calculated in the same way:

$$(x_1', y_1', z_1')^T = R_1\left(x, y, z + h_{(x,y)}\right)^T + T_1 \tag{6}$$

$$(x_2', y_2', z_2')^T = R_2\left(x, y, z + h_{(x,y)}\right)^T + T_2 \tag{7}$$

$$(u_1', v_1', 1)^T = K_1\left(\frac{x_1'}{z_1'}, \frac{y_1'}{z_1'}, 1\right)^T \tag{8}$$

$$(u_2', v_2', 1)^T = K_2\left(\frac{x_2'}{z_2'}, \frac{y_2'}{z_2'}, 1\right)^T \tag{9}$$

$$\varphi_{2(x,y,z+h_{(x,y)})} = \left(\frac{2\pi u_1'}{p_1} + \varphi_{10}\right) - \left(\frac{2\pi u_2'}{p_2} + \varphi_{20}\right). \tag{10}$$

The change in the phase caused by $h\,(x, y)$ is

$$\Delta\varphi_{(x,y,z,h_{(x,y)})} = \frac{2\pi}{p_1}\,(u_1' - u_1) - \frac{2\pi}{p_2}\,(u_2' - u_2)\,. \tag{11}$$

When the reference plane coincides with the $Z = 0$ plane, the out-of-plane displacement equals to the height. Substituting all intermediate variables, u_1, u_1', u_2, u_2', into equation (11) with the corresponding expressions of x, y, h, we obtain

$$\begin{aligned}
&\Delta\varphi_{(x,y,h_{(x,y)})} \\
&= \frac{2\pi K_{111}}{p_1}\left[\frac{R_{111}x+R_{112}y+R_{113}h_{(x,y)}+T_{11}}{R_{131}x+R_{132}y+R_{133}h_{(x,y)}+T_{13}} - \frac{R_{111}x+R_{112}y+T_{11}}{R_{131}x+R_{132}y+T_{13}}\right] \\
&+ \frac{2\pi K_{112}}{p_1}\left[\frac{R_{121}x+R_{122}y+R_{123}h_{(x,y)}+T_{12}}{R_{131}x+R_{132}y+R_{133}h_{(x,y)}+T_{13}} - \frac{R_{121}x+R_{122}y+T_{12}}{R_{131}x+R_{132}y+T_{13}}\right] \\
&- \frac{2\pi K_{211}}{p_2}\left[\frac{R_{211}x+R_{212}y+R_{213}h_{(x,y)}+T_{21}}{R_{231}x+R_{232}y+R_{233}h_{(x,y)}+T_{23}} - \frac{R_{211}x+R_{212}y+T_{21}}{R_{231}x+R_{232}y+T_{23}}\right] \\
&- \frac{2\pi K_{212}}{p_2}\left[\frac{R_{221}x+R_{222}y+R_{223}h_{(x,y)}+T_{22}}{R_{231}x+R_{232}y+R_{233}h_{(x,y)}+T_{23}} - \frac{R_{221}x+R_{222}y+T_{22}}{R_{231}x+R_{232}y+T_{23}}\right].
\end{aligned} \tag{12}$$

$K_{ijk}(i = 1, 2; j = 1, 2; k = 1, 2)$ is the element in the jth row and kth column of matrix K_i, $R_{ijk}(i = 1, 2; j = 1, 2, 3; k = 1, 2, 3)$ is the element in the jth row and kth column of matrix R_i, and $T_{ij}(i = 1, 2; j = 1, 2, 3)$ is the jth element of vector T_i.

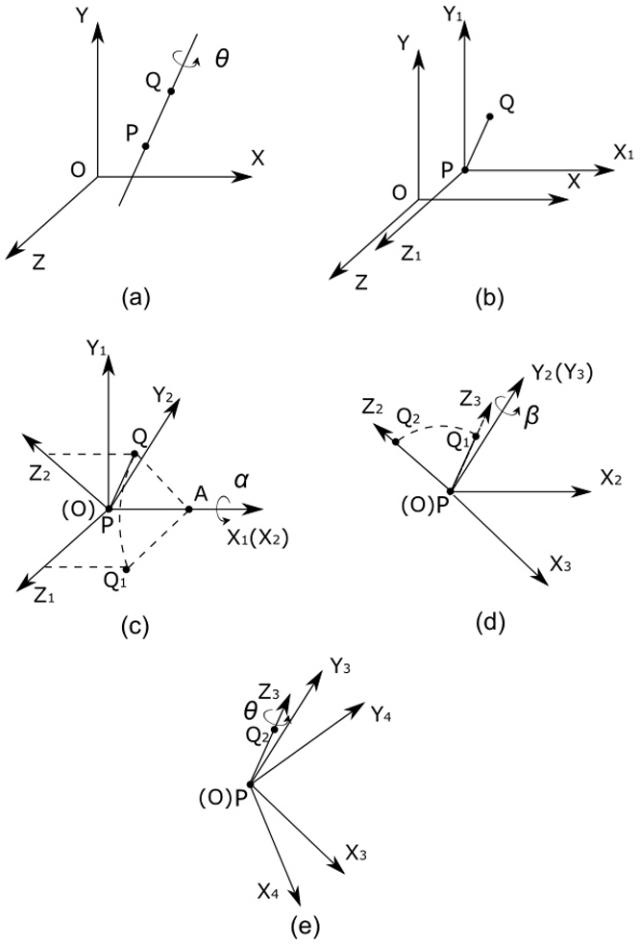

Figure 3. (a) An arbitrary axis rotation transformation, (b) translation of coordinate system, (c) rotation around the X coordinate axis, (d) rotation around the Y coordinate axis, (e) rotation around the Z coordinate axis.

Equation (12) is a universal formula that expresses the relationship between the phase difference $\Delta\varphi_{(x,y,h_{(x,y)})}$ and height $h\,(x, y)$, for a generic optical setup. Using the four-step phase shifting method, it is easy to calculate the whole field's phase maps and phase difference $\Delta\varphi_{(x,y,h_{(x,y)})}$. $h\,(x, y)$ can be worked out using an iterative numerical algorithm after system calibration.

2.2. Rotation scanning projection moiré technique

Figure 2 shows two typical types of rotation scanning projection moiré system: (a) the single-axis mode with a projection system and a receiving system placed on the same turntable; and (b) the dual-axis mode with a projection system and a receiving system placed on two turntables. The basic projection moiré method still works in the rotation scanning projection moiré system. The main problem that needs to be solved is how to calculate the system parameters of the system after rotation. Driven by the desire to keep the rotation scanning system simple, the two main parts of the rotation scanning projection moiré system, namely the projecting system and the receiving system, can be considered as one block whose components and configurations do not change during experiments.

Table 1. System parameters before and after rotation.

Initial	Projection system: $\overrightarrow{P_1Q_1}\ \theta_1$ Receiving system: $\overrightarrow{P_2Q_2}\ \gamma_1$	Projection system: $\overrightarrow{P_1Q_1}\ \theta_2$ Rotation system: $\overrightarrow{P_2Q_2}\ \gamma_2$
R_1	$R_{11}=\overline{R}_{(x_{01},y_{01},z_{01},a_1,b_1,c_1,\theta_1)}R_1$	$R_{12}=\overline{R}_{(x_{01},y_{01},z_{01},a_1,b_1,c_1,\theta_2)}R_1$
T_1	$T_{11}=\overline{R}_{(x_{01},y_{01},z_{01},a_1,b_1,c_1,\theta_1)}T_1+\overline{T}_{(x_{01},y_{01},z_{01},a_1,b_1,c_1,\theta_1)}$	$T_{12}=\overline{R}_{(x_{01},y_{01},z_{01},a_1,b_1,c_1,\theta_2)}T_1+\overline{T}_{(x_{01},y_{01},z_{01},a_1,b_1,c_1,\theta_2)}$
K_1	K_1	K_1
R_2	$R_{21}=\overline{R}_{(x_{02},y_{02},z_{02},a_2,b_2,c_2,\gamma_1)}R_2$	$R_{22}=\overline{R}_{(x_{02},y_{02},z_{02},a_2,b_2,c_2,\gamma_2)}R_2$
T_2	$T_{21}=\overline{R}_{(x_{02},y_{02},z_{02},a_2,b_2,c_2,\gamma_1)}T_2+\overline{T}_{(x_{02},y_{02},z_{02},a_2,b_2,c_2,\gamma_1)}$	$T_{22}=\overline{R}_{(x_{02},y_{02},z_{02},a_2,b_2,c_2,\gamma_2)}T_2+\overline{T}_{(x_{02},y_{02},z_{02},a_2,b_2,c_2,\gamma_2)}$
K_2	K_2	K_2

Overall, there are four fundamental transformations, one translation and three rotations around different coordinate axes:

$$\begin{pmatrix}x'\\y'\\z'\end{pmatrix}=\begin{pmatrix}x\\y\\z\end{pmatrix}-\begin{pmatrix}a\\b\\c\end{pmatrix} \tag{13}$$

$$\begin{pmatrix}x'\\y'\\z'\end{pmatrix}=\begin{pmatrix}1&0&0\\0&\cos\alpha&\sin\alpha\\0&-\sin\alpha&\cos\alpha\end{pmatrix}\begin{pmatrix}x\\y\\z\end{pmatrix} \tag{14}$$

$$\begin{pmatrix}x'\\y'\\z'\end{pmatrix}=\begin{pmatrix}\cos\beta&0&-\sin\beta\\0&1&0\\\sin\beta&0&\cos\beta\end{pmatrix}\begin{pmatrix}x\\y\\z\end{pmatrix} \tag{15}$$

$$\begin{pmatrix}x'\\y'\\z'\end{pmatrix}=\begin{pmatrix}\cos\theta&\sin\theta&0\\-\sin\theta&\cos\theta&0\\0&0&1\end{pmatrix}\begin{pmatrix}x\\y\\z\end{pmatrix}. \tag{16}$$

We denote the four fundamental transformations as $T\begin{pmatrix}a & b & c\end{pmatrix}$, $R_X(\alpha)$, $R_Y(\beta)$, and $R_Z(\theta)$.

Any complex coordinate transformation could be separated into a series of fundamental transformations. Considering the coordinate system rotates about an arbitrary rotation axis, the rotation angle θ is given, as well as all of the parameters of the rotation axis PQ including position information $P\begin{pmatrix}x_0 & y_0 & z_0\end{pmatrix}^T$ and direction information $\overrightarrow{PQ}=\begin{pmatrix}a & b & c\end{pmatrix}^T$. The transformation can be separated into seven steps.

(1) Translate the coordinate system and make the origin coincide with P, denoted as $T\begin{pmatrix}x_0 & y_0 & z_0\end{pmatrix}$.
(2) Rotate the coordinate system around the X coordinate axis and make the rotation axis in the XOY plane, denoted as $R_X(\alpha)$. The rotation angle α is determined by $\sin\alpha=-\frac{b}{\sqrt{b^2+c^2}}$, $\cos\alpha=\frac{c}{\sqrt{b^2+c^2}}$.
(3) Rotate the coordinate system around the Y coordinate axis and make the rotation axis coincide with the Z coordinate axis, denoted as $R_Y(\beta)$. The rotation angle β is determined bysin $\beta=-\frac{a}{\sqrt{a^2+b^2+c^2}}$, $\cos\beta=\frac{\sqrt{b^2+c^2}}{\sqrt{a^2+b^2+c^2}}$.
(4) Rotate the coordinate system around the Z coordinate axis, denoted as $R_Z(\theta)$. θ is the rotation angle.

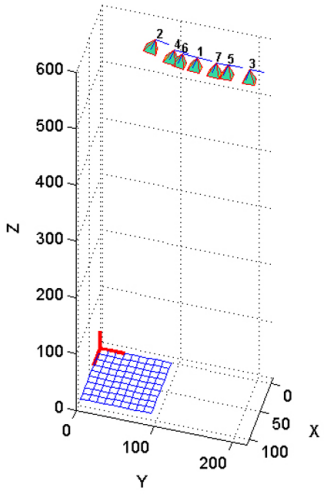

Figure 4. Schematic plot of rotation axis calibration.

(5) Apply the inverse transformation of Step 3, denoted as $R_Y(-\beta)$.
(6) Apply the inverse transformation of Step 2, denoted as $R_X(-\alpha)$.
(7) Apply the inverse transformation of Step 1, denoted as $T\begin{pmatrix}-x_0 & -y_0 & -z_0\end{pmatrix}$.

Figure 3 shows the first four transformations. According to these seven transformations, the coordinate transformation M after the coordinate system rotating around an arbitrary axis could be worked out from the following equation:

$$\begin{aligned}M=&T\begin{pmatrix}-x_0 & -y_0 & -z_0\end{pmatrix}R_X(-\alpha)R_Y(-\beta)R_Z(\theta)\\&R_Y(\beta)R_X(\alpha)T\begin{pmatrix}x_0 & y_0 & z_0\end{pmatrix}.\end{aligned} \tag{17}$$

The coordinates before and after the rotation has the relation as follows:

$$\begin{pmatrix}x'\\y'\\z'\end{pmatrix}=\overline{R}_{(x_0,y_0,z_0,a,b,c,\theta)}\begin{pmatrix}x\\y\\z\end{pmatrix}+\overline{T}_{(x_0,y_0,z_0,a,b,c,\theta)} \tag{18}$$

where

$$\begin{aligned}\overline{R}_{(x_0,y_0,z_0,a,b,c,\theta)}&=R_X(-\alpha)R_Y(-\beta)R_Z(\theta)R_Y(\beta)R_X(\alpha)\\\overline{T}_{(x_0,y_0,z_0,a,b,c,\theta)}&=T\begin{pmatrix}x_0 & y_0 & z_0\end{pmatrix}-\overline{R}_{(x_0,y_0,z_0,a,b,c,\theta)}T\begin{pmatrix}x_0 & y_0 & z_0\end{pmatrix}.\end{aligned} \tag{19}$$

x_0, y_0, z_0, a, b, c, θ are rotation parameters.

Considering that the single-axis mode could be seen as a special case of the dual-axis mode in which the two rotation stages share a rotation axis, the theory for the dual-axis mode can also be applied to the single-axis mode. We are going to discuss parameter calculation in the dual-axis mode. Given the system parameters before the rotation, as well as related rotation parameters, it is possible to work out the extrinsic system parameters after rotation, using the coordinate transformation formulas as above.

Take the projection system as an example. Considering an arbitrary point $A\,(x, y, z)$, its coordinates in the coordinate system $O_1X_1Y_1Z_1$ is (x_1, y_1, z_1):

$$(x_1, y_1, z_1)^T = R_1(x, y, z)^T + T_1. \tag{20}$$

If the coordinate system rotates around an axis by a certain angle, all of the rotation parameters $x_{01}, y_{01}, z_{01}, a_1, b_1, c_1, \theta_1$ are known. According to equation (18), the coordinate of point A after the rotation is

$$\begin{pmatrix} x_1' & y_1' & z_1' \end{pmatrix}^T = \overline{R}_{(x_{01},y_{01},z_{01},a_1,b_1,c_1,\theta_1)}(x_1, y_1, z_1)^T + \overline{T}_{(x_{01},y_{01},z_{01},a_1,b_1,c_1,\theta_1)}. \tag{21}$$

Substituting equation (20) in (21):

$$\begin{pmatrix} x_1' & y_1' & z_1' \end{pmatrix}^T = R_{11}(x, y, z)^T + T_{11}$$

$$R_{11} = \overline{R}_{(x_{01},y_{01},z_{01},a_1,b_1,c_1,\theta_1)}R_1$$

$$T_{11} = \overline{R}_{(x_{01},y_{01},z_{01},a_1,b_1,c_1,\theta_1)}T_1 + \overline{T}_{(x_{01},y_{01},z_{01},a_1,b_1,c_1,\theta_1)}. \tag{22}$$

Because the components and configurations in the projection system do not change during the rotation, the internal parameter K_1 can be seen as a constant matrix. Only the external parameters will change after the rotation: R_1, T_1 will change into R_{11}, T_{11}. Equation (22) provides the formulas for their calculation.

If the projection system rotates by another angle, θ_2, the exterior parameters, R_{12} and T_{12}, can be worked out in the same way:

$$\begin{pmatrix} x_1'' & y_1'' & z_1'' \end{pmatrix}^T = R_{12}(x, y, z)^T + T_{12}$$

$$R_{12} = \overline{R}_{(x_{01},y_{01},z_{01},a_1,b_1,c_1,\theta_2)}R_1$$

$$T_{12} = \overline{R}_{(x_{01},y_{01},z_{01},a_1,b_1,c_1,\theta_2)}T_1 + \overline{T}. \tag{23}$$

Similarly, if the receiving system rotates around another axis, the parameters of this axis, $x_{02}, y_{02}, z_{02}, a_2, b_2, c_2$, are known, as well as two different rotation angles γ_1, γ_2, and the coordinate transformations are as follows:

$$\begin{pmatrix} x_2' & y_2' & z_2' \end{pmatrix}^T = R_{21}(x, y, z)^T + T_{21}$$

$$R_{12} = \overline{R}_{(x_{01},y_{01},z_{01},a_1,b_1,c_1,\theta_2)}R_1 \tag{24}$$

$$T_{21} = \overline{R}_{(x_{02},y_{02},z_{02},a_2,b_2,c_2,\gamma_1)}T_2 + \overline{T}_{(x_{02},y_{02},z_{02},a_2,b_2,c_2,\gamma_1)}$$

$$\begin{pmatrix} x_2'' & y_2'' & z_2'' \end{pmatrix}^T = R_{22}(x, y, z)^T + T_{22}$$

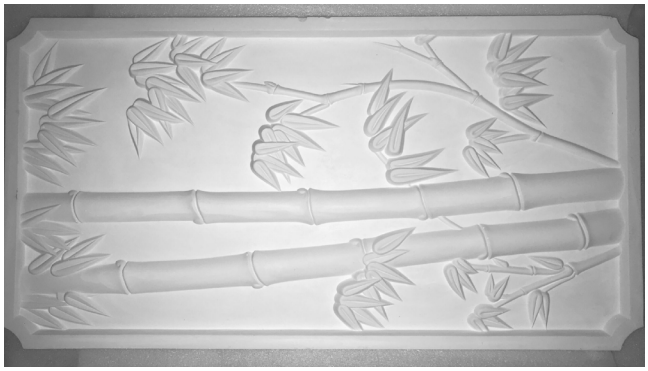

Figure 5. Gypsum plate with bamboo design.

$$R_{12} = \overline{R}_{(x_{01},y_{01},z_{01},a_1,b_1,c_1,\theta_2)}R_1$$

$$T_{22} = \overline{R}_{(x_{02},y_{02},z_{02},a_2,b_2,c_2,\gamma_2)}T_2 + \overline{T}_{(x_{02},y_{02},z_{02},a_2,b_2,c_2,\gamma_2)}. \tag{25}$$

In general, if the object's 3D surface reconstruction needs to be conducted from three different measurement angles, we take the two positions in the middle as the 0° position for each system, as shown in figure 2(b). The rotation angles for the projection system and the receiving system are θ_1, θ_2, γ_1, γ_2, also marked in figure 2(b). Summarizing equations (22)–(25), the changed exterior parameters can be calculated; these are listed in table 1. The first column lists the system parameters when the projection system and receiving system are at their initial positions. Column 2 and Column 3 list system parameters after the two systems are rotated to different positions. However, a precondition is that rotation parameters need to be calibrated. Actually, calibration of rotation parameters can be conducted at the same time as the camera and projector calibrations. The latter is needed because a calibration board is moved and the board's image is captured from several different orientations. If the calibration board is fixed, the camera can be rotated to different positions for image acquisition, which is equivalent to fixing the camera and rotating the calibration board around the same axis. Thus, the axis could be fitted out with those grid points' discrete circular tracing points.

3. Experiment

To validate our approach, we conducted an experiment using the dual-axis mode for measuring a gypsum plate from three different directions. Before that, system parameters should be calibrated in the first place, including camera intrinsic parameter, extrinsic parameter, as well as two rotation axes' parameters.

3.1. System calibration

Zhang's method [22] is fast, simple, and most widely applied. The calibration process only needs to take a few picures of a calibration board from different orientations by moving either the calibration board or camera. Both the intrisic and extrinsic

Table 2. Parameters of the rotation scanning projection moiré system.

	Projector	Receiving system
Intrinsic parameter	$K_1 = \begin{pmatrix} 3865.2 & 0 & 959.5 \\ 0 & 3852.3 & 599.5 \\ 0 & 0 & 1 \end{pmatrix}$	$K_2 = \begin{pmatrix} 2283.1 & 0 & 830.4 \\ 0 & 2281.2 & 782.9 \\ 0 & 0 & 1 \end{pmatrix}$
Extrinsic parameter	$R_1 = \begin{pmatrix} 0.0158 & 0.9766 & 0.2145 \\ 0.9953 & 0.0052 & -0.0969 \\ -0.0957 & 0.2150 & -0.9719 \end{pmatrix}$	$R_2 = \begin{pmatrix} 0.0123 & 0.9876 & -0.1283 \\ 0.9998 & -0.0104 & 0.0155 \\ 0.0140 & -0.1285 & -0.9916 \end{pmatrix}$
	$T_1 = \begin{pmatrix} -9.2 \\ -30.6 \\ 889.7 \end{pmatrix}$	$T_2 = \begin{pmatrix} -29.4 \\ -60.4 \\ 745.7 \end{pmatrix}$
Rotation parameter	$\begin{pmatrix} x_{01} \\ y_{01} \\ z_{01} \end{pmatrix} = \begin{pmatrix} 3.0 \\ 0 \\ 153.6 \end{pmatrix}$	$\begin{pmatrix} x_{02} \\ y_{02} \\ z_{02} \end{pmatrix} = \begin{pmatrix} 26.8 \\ 0 \\ -108.2 \end{pmatrix}$
	$\begin{pmatrix} a_1 \\ b_1 \\ c_1 \end{pmatrix} = \begin{pmatrix} -0.0017 \\ 1 \\ -0.0003 \end{pmatrix}$	$\begin{pmatrix} a_2 \\ b_2 \\ c_2 \end{pmatrix} = \begin{pmatrix} -0.0001 \\ 1 \\ -0.0002 \end{pmatrix}$

Table 3. Rotation angles of the projection system and the receiving system.

	Status 1	Status 2	Status 3
Projection system/°	0	7	−8
Receiving system/°	0	8	−7

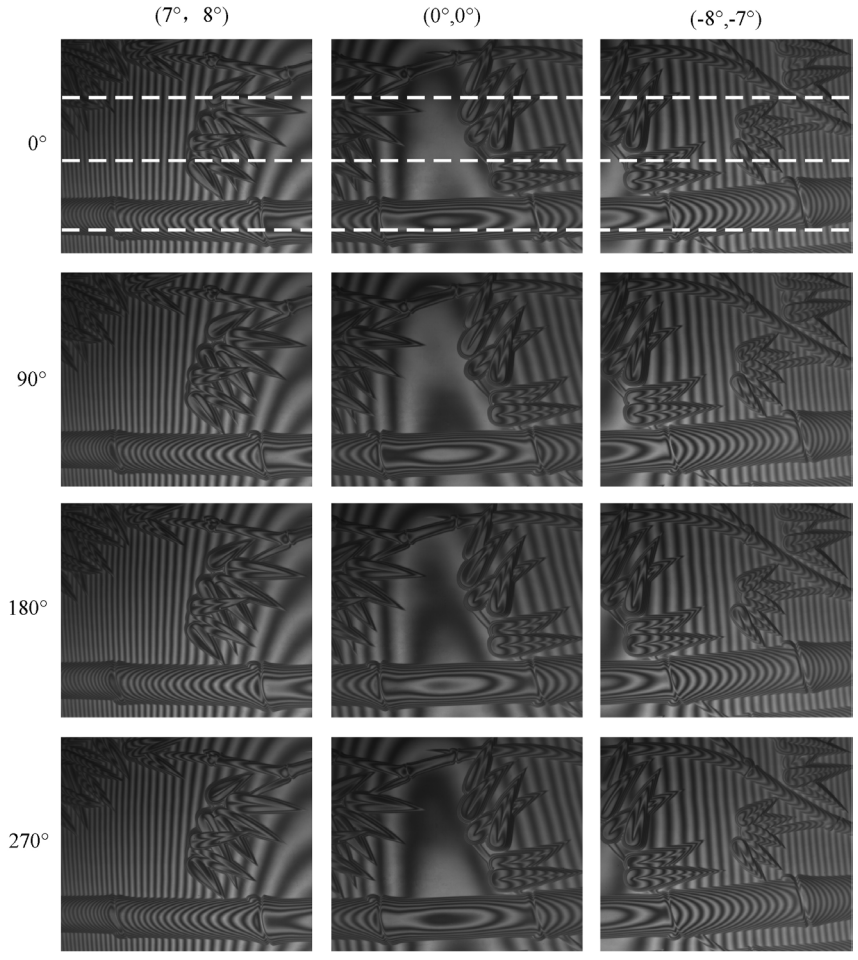

Figure 6. Four-step phase shifting moiré patterns of the gypsum plate.

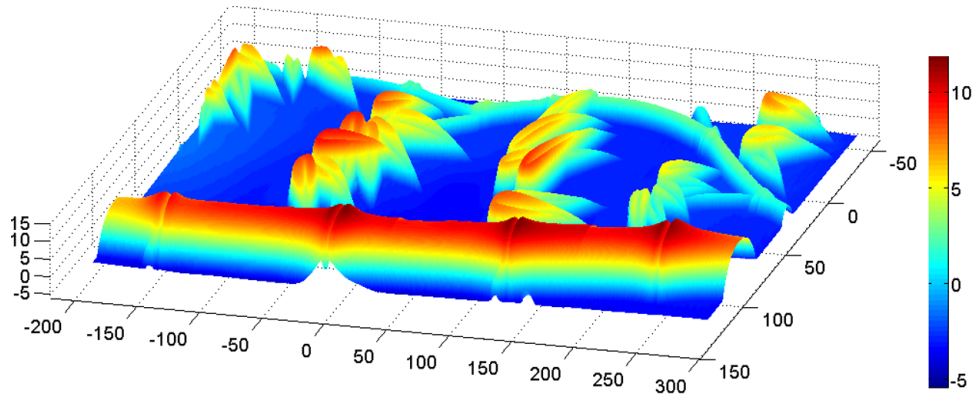

Figure 7. Reconstruction result for the gypsum plate.

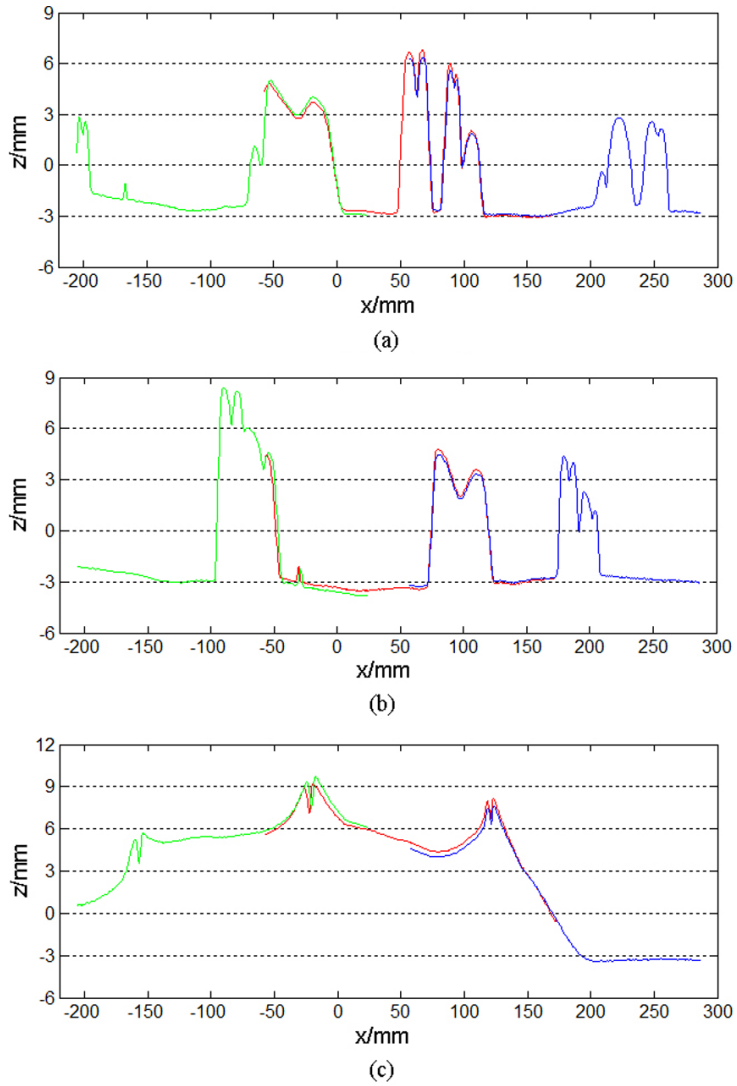

Figure 8. Height curves of the 3D surface measurement result for the gypsum plate: (a) the 100th row, (b) the 210th row, (c) the 330th row.

parameters could be worked out, as well as corner points' coordinates under different orientations.

In a projection moiré system, the receiving system could be seen as a whole, like a camera, and the projector also could be seen as an inverse camera. Both of them could be calibrated using Zhang's method. The intrinsic and extrinsic parameters in the initial position are listed in table 2. Please refer to [21] for more details.

The rotation parameter means the rotation axes' position and direction. We fix the calibration board, rotate the projector and receiving system, and take a few pictures. Figure 4 shows the calibration board and seven positions of the projector.

Table 4. Measurement error of translation experiment.

Translation/mm		5.00	10.00
Status 1	Ave/mm	5.02	9.99
	Relative/%	0.4	0.1
	RMS/mm	0.009	0.015
Status 2	Ave/mm	4.96	9.87
	Relative/%	0.8	1.3
	RMS/mm	0.012	0.020
Status 3	Ave/mm	4.85	9.71
	Relative/%	3.0	2.9
	RMS/mm	0.024	0.035

Note: 'Ave' is the average height value of the plane. 'Relative' is 'relative error' of the average height compared to the theoretical value. RMS is the 'root mean square error'.

Rotation parameters can be worked out by fitting arc locus. The rotation parameters are also listed in table 2.

3.2. Measurement experiment

The gypsum plate's dimensions were 800 mm × 420 mm; the plate is shown in figure 5. The rotation angles of the projection system and the receiving system for the different measuring statuses are listed in table 3. Figure 6 shows the moiré patterns of the gypsum plate during the experiment. The measurement area for each status was about 200 mm × 180 mm. The white dotted lines are three randomly picked lines; their height curves will be discussed later.

The result of the reconstruction is shown in figure 7. By combining the measurement results for the three statuses, we obtain a 480 mm × 180 mm reconstructed surface. For more details, we drew three lines across the reconstructed surface and show the height curves in figure 8. The real error is the difference between the results for the different view-angles of the same point, but it is not very difficult to find each point's corresponding point. The height curve in figure 8 can only tell the Z coordinate error from different view-angles. The maximal error of the Z coordinate is ~0.5 mm.

Generally, if we want to discuss measurement error, the real value is needed as a reference. In our experiment, we measured a complex unknown surface; it is difficult to ascertain the exact coordinate information. So we conduct another experiment using the same method. Firstly, we measure the surface of a planar board. Then, we translate the board twice toward projection moiré system and measure its surface, 5 mm at a time. Table 4 gives the measurement error of the translation experiment. The error of status 1 is smaller than the other two status. It is completely comprehensible. Status 1 is the initial position, where the extrinsic parameters $R_1$and T_1 are calibrated. They are more accurate than the extrinsic parameters of statuses 2 and 3 calculated from rotation axis and rotation angle.

4. Conclusion

This paper presented a rotation scanning projection moiré method for 3D surface reconstruction. We derived the system parameters' transformation equations after rotation; thus, all system parameters can be worked out in the circumstance of pure rotation for the projection system and the receiving system. Measurements can be completed using the new set of system parameters. In this way, the measurement area increases. The experiment confirms the feasibility and validity of the proposed method. The measurement area increased from 200 mm × 180 mm to 480 mm × 180 mm. The biggest RMS error is about 0.035 mm. But this method has its limitations, too. Since the projection moiré method is based on moiré phases, so the measurement area is limited by high-quality imaging by camera.

Acknowledgments

This work is supported by National Natural Science Foundation of China (NSFC) under Grant No. 11732009.

ORCID iDs

Jubing Chen https://orcid.org/0000-0003-3023-3959

References

[1] Meadows D M, Johnson W O and Allen J B 1970 Generation of surface contours by moiré patterns *Appl. Opt.* **9** 942
[2] Takasaki H 1970 Moiré topography *Appl. Opt.* **9** 1467
[3] Nomura T and Shinomura K 2017 Generalized sequential four-step phase-shifting color digital holography *Appl. Opt.* **56** 6851
[4] Song Y, Chen Y, Wang J, Sun N and He A 2012 Four-step spatial phase-shifting shearing interferometry from moiré configuration by triple gratings *Opt. Lett.* **37** 1922
[5] Choi Y B and Kim S W 1998 Phase-shifting grating projection moiré topography *Opt. Eng.* **37** 1005
[6] Ghiglia D C and Romero L A 1994 Robust two-dimensional weighted and unweighted phase unwrapping that uses fast transforms and iterative methods *J. Opt. Soc. Am.* A **11** 107
[7] Abdul-Rahman H S, Gdeisat M A, Burton D R, Lalor M J, Lilley F and Moore C J 2007 Fast and robust three-dimensional best path phase unwrapping algorithm *Appl. Opt.* **46** 6623
[8] Zhao M, Huang L, Zhang Q, Su X, Asundi A and Qian K 2011 Quality-guided phase unwrapping technique: comparison of quality maps and guiding strategies *Appl. Opt.* **50** 6214

[9] Boccaccio A, Martino F and Pappalettere C 2015 A novel moiré-based optical scanning head for high-precision contouring *Int. J. Adv. Manuf. Technol.* **80** 47
[10] Sciammarella C A, Lamberti L and Sciammarella F M 2005 High accuracy contouring using projection moiré *Opt. Eng.* **44** 093605
[11] Fleming G A, Bartram S M, Waszak M R and Jenkins L N 2001 Projection moiré interferometry measurements of micro air vehicle wings *Proc. SPIE* **4448** 90
[12] Dirckx J J J and Decraemer W F 1997 Optoelectronic moiré projector for real-time shape and deformation studies of the tympanic membrane *J. Biomed. Opt.* **2** 176
[13] Laulund T, Søjbjerg J O and Hørlyck E 1982 Moiré topography in school screening for structural scoliosis *Acta Orthopaedica Scandinavica* **53** 765
[14] Ramulu M, Labossiere P and Greenwell T 2010 Elastic–plastic stress/strain response of friction stir-welded titanium butt joints using moiré interferometry *Opt. Lasers Eng.* **48** 385
[15] Cosola E, Genovese K, Lamberti L and Pappalettere C 2008 A general framework for identification of hyper-elastic membranes with moiré techniques and multi-point simulated annealing *Int. J. Solids Struct.* **45** 6074
[16] Wang Q, Tsuda H and Xie H 2015 Developments and applications of moire techniques for deformation measurement, structure characterization and shape analysis *Recent Patents Mater. Sci.* **8** 188
[17] Nguyen H, Nguyen D, Wang Z, Kieu H and Le M 2015 Real-time, high-accuracy 3d imaging and shape measurement *Appl. Opt.* **54** A9
[18] Cubero S and Blasco J 2011 Advances in machine vision applications for automatic inspection and quality evaluation of fruits and vegetables *Food Bioprocess Technol.* **4** 487
[19] Mcpherron S P, Gernat T and Hublin J J 2009 Structured light scanning for high-resolution documentation of in situ archaeological finds *J. Archaeol. Sci.* **36** 0
[20] Ma L, Xu T and Lin J 2009 Validation of a three-dimensional facial scanning system based on structured light techniques *Comput. Methods Prog. Biomed.* **94** 290
[21] Tang Y, Yao J, Zhou Y, Sun C, Yang P, Miao H and Chen J 2017 Calibration of an arbitrarily arranged projection moiré system for 3D shape measurement *Opt. Lasers Eng.* **104** 135
[22] Zhang Z 1999 Flexible camera calibration by viewing a plane from unknown orientations *Proc. 7th IEEE Int. Conf. on Computer Vision* vol 22 p 1330